

Mine Detection Robot and Related Technologies for Humanitarian Demining

Kenzo Nonami*, Seiji Masunaga*, Daniel Waterman*
Hajime Aoyama**, and Yoshihiro Takada**

**Chiba University
Japan*

***Fuji Heavy Industries
Japan*

1. Introduction

Currently, more than 100 million anti-personnel mines are under the ground all over the world. These mines not only disturb the economic development of mine-buried nations, but also injure or kill more than 2000 people a month. As a result, the removal of landmines has become a global emergency. The current method of removing mines manually is costly and dangerous. Moreover, removal of all mines by this method would require several hundred years (it would take one thousand according to a CMAC report based on Cambodian Mine Action Center Current Activities 1998), during which time, more mines might be buried in war zones.

There are three kinds of demining strategies. The first is human deminer based demining. The second is mechanical equipment based demining like Fig.1(Geneva International Center for Humanitarian Demining,2002). The third is advanced robot based demining. Currently, the most common demining approach is the first type. The second type is applied in some limited mine field area. The third type is partially tried as mine detection or brush cutting with the exception of research oriented robots and some of them will be expected in future demining approaches. Figure 2 shows the robotic brush cutter which was developed in the Demining Technology Workshop in Cambodia. This robot can cut grass and bush by teleoperation.

Figure 3 shows the four legged mine detection robot which was studied by CSIC-IAI, Spain in 1999(Armada et al.2005). Under this extreme environment, a walking robot may be an effective and efficient means of detecting and removing mines while ensuring the safety of local residents and people engaged in the removal work. The six-legged and crawler type hybrid robot COMET-III(Nonami et al.2003) shown in Fig.4 with two manipulators based on the added stability, mobility, and functionality that this platform offers. This latest robot COMET-III, which is fully autonomous, has been developed by one of this paper's authors.

Source: Humanitarian Demining: Innovative Solutions and the Challenges of Technology. Book edited by: Maki K. Habib, ISBN 978-3-902613-11-0, pp. 392, February 2008, I-Tech Education and Publishing, Vienna, Austria



Fig. 1. Mechanical demining equipment



Fig. 2. Tempest for brush cutter



Fig. 3. Four legged mine detection robot



Fig. 4. Mine detection robot COMET-III

The total weight is about 1000kg, the size is 4m long, 2.5m wide, and 0.8m high. The COMET-III has 40 liter gasoline tank to continuously work for 4 hours and 700cc gasoline engine like an automobile engine to generate DC power supply and to drive the hydraulic motor. So, the driving force is based on hydraulic power with 14 MPa high pressure and the total power is 25PS. The walking speed on six legs is about 300m/h and the running speed by rubber crawler is 4km/h. Therefore, the COMET-III is a hybrid system and it has two manipulators which are used for mine detection and marking. Also it has a 3D stereo vision camera to make online mapping and trajectory planning, so the COMET-III can be called a fully autonomous mine detection robot. This kind of robot is the third type of demining strategy, based on advanced robotics, and is the future's approach.

Currently our group is participating in the Japan Science and Technology Agency's (JST) Sensing and Access Control R&D for Humanitarian Mine Action project with our effort to develop a small vehicle for mine detection and clearance. This small vehicle is named Mine Hunter Vehicle (MHV). Specifically we were concerned with the development of a 4 degree-of-freedom robot arm which is called as SCARA arm for sensing buried anti-personnel mines. We have divided the project into several tasks to be tackled. Our team, in cooperation with Fuji Heavy Industries and Sato's group from Tohoku University, and Arai's group from University of Electro-Communications has proposed a small teleoperated vehicle-based system. The task of landmine detection is being undertaken by Sato's group at Tohoku University, who are developing an array-style ground penetrating radar (SAR-

GPR). Our group including Fuji Heavy Industries is responsible for the development and control of an arm that the sensor will be mounted on and the mine clearance manipulator.

2. State of the art of Teleoperated Mine Detection by Vehicle Mounted Mine Detector

Conventional vehicle-mounted mine detector systems employ an array of sensors elements to achieve a detection swath typically 2~4m wide. Some systems employ more than one type of sensor technology. These systems, while being very useful are often expensive, complex and inflexible. A human operator, on the other hand, sweeps a mine detector from side to side while moving forward to cover ground. The operator can follow the ground profile with the detector head close to the ground without hitting the ground or any objects on it. The operator can also vary the wide of sweep to suit a particular situation, and is usually not limited by terrain. However the manual method is slow, harzardous, manpower-intensive, and stressful to the operation who, as a result, can perform this task only for short periods at a time. As well, the task is monotonous and at times errors result due to operator inattentiveness.

Canadian Center for Mine Action Technologies (CCMAT) developed the robotic scanner shown in Fig.5 which uses a robotic device capable of autonomously moving a mine detection sensor over natural ground surfaces including roads and tracks in a manner similar to a human operator. Such a device, operated remotely, will increase the safety of the personnel performing mine detection. As well, this will provide a more flexible and less expensive way of sweeping surfaces such as roads and fields than systems which employ a static array of a vehicle-mounted systems. Although several vehicle-mounted systems are protected against conventional antitank mines, they still may require a precursor vehicle to neutralize antipersonnel and tilt-rod mines. For the system proposed by CCMAT, the requirement for protection will be much reduced primarily because mines will be detected ahead of the vehicle without the sensor contacting the ground.

Figure 6 shows the vehicle mounted mine detector (VMMD). The VMMD is a modified small utility vehicle. The VMMD sensor package consists of Ground Penetrating Radar (GPR) and infrared and ultraviolet cameras. The VMMD did well in detecting antitank mines, but had difficulty identifying antipersonnel mines and proved very complicated to operate.

Figure 7 shows the semi-autonomous mine detection system (SAMS). The SAMS is designed to reduce the threat to deminers by remotely detecting, marking and allows towing of a Sciebel Metal Detection Array. SAMS can remotely navigate into minefields to detect, mark, and map buried mines using a metal detection array and differential GPS position location equipment under semi-autonomous remote control.



Fig. 5. Robotic Scanner mounted on teleoperated vehicle[5]



Fig. 6. Vehicle Mine Detector (VMMD)[6]

Figure 8 shows another Vehicle Mounted Detection System (VMDS). The VMDS concept is based on a commercial skid steer chassis modified to incorporate a remote control capability. The VMDS sensor package consists of a 2m wide Sciebel metal detection array, a Thermal-Neutron Analysis (TNA) sensor, and an infrared sensor. The 2meter array detects metal objects in the vehicle's path, while the TNA indicates those targets that contain explosive. In testing, the 2meter detection array performed extremely well. The TNA found most AT mines, but had difficulty identifying AP mines and proved very complicated to operate.

3. Concept and Implementation of Mine Hunter Vehicle (MHV)

As above mentioned, our group was participating in the JST Sensing and Access Control R&D for Humanitarian Mine Action project with our effort to develop a small vehicle for mine detection and clearance. This small vehicle is named Mine Hunter Vehicle (MHV) and is equipped with mine detection sensors. The general design considerations were as follows;

- (1) A robot that can be loaded into 2 ton vehicles.
- (2) Division is easy.
- (3) The weight of the main part of the vehicles is 1100kg - 1500kg.
- (4) It has an environment-proof nature, able to carry out a certain operation in the climate of Afghanistan.
- (5)The vehicle can climb up and down slopes in mountain regions.
- (6)The vehicle has durability against blasts from antipersonnel mines.
- (7)A reliable control device should be developed.
- (8)Both front detection and side detection are possible.

The design specification of the main body of MHV was as follows;

- (1) Simple body structure
- (2)45-degree slope climbing capability, and spin turn.
- (3)Durability and reliability test of an engine system, a drive system, and axle part
- (4)Development of the axle which can easily fitted with crawlers or tires
- (5)Durability and reliability test of bulletproof equipment of an anti-personnel mine level

- (6) Durability and reliability test of the protection-against-dust nature which prevents invasion of minute sand etc. into flexible regions
- (7) Development of a reliable controller, a remote control, and image transmission equipment

The body full length of MHV is 2.8m, and when the sensor arm is lengthened, it is 4.5m. The width of vehicle is 1.5m in the case of crawler, and is 1.6m in the tire. The height of vehicles is 1.9m in the crawler, and is 1.8m in the tire. The full weight is 1650kg including SCARA arm. The drive is a diesel engine and a HST (Hydraulic Static Transmission) system. Four independent crawlers are attached to the front right, the front left, the back right, and the back left. The engine was selected to be applicable to the 2,000m high elevation in Afghanistan. The left-hand side crawler (front, rear) and right-hand side crawler (front, rear) have a separate hydraulic pump and the hydraulic circuits are independent of each other. Furthermore, MHV crawlers can rotate in ± 25 degrees centering on an axle. Because of this reason, the slip of the crawlers on road surfaces decreased and it became easier to negotiate irregular ground and ascend and descend sloped ground. Changing between crawlers and tires can be done easily by removing eight bolts, like changing a tire of a normal car. A high-strength steel plate of 4.5mm was attached in front with the bolts. The rotation part of the axles are bush bearings strong against shock and do not require lubrication, however in order to prevent sand and dust from invading the bearings, oil seals are attached to both sides. Even if the axles are submerged in water, there will be no leak.

The control device consists of modules which include the controller for hydraulic pressure, a proportionality electromagnetic valve driver, a remote control, image transmission equipment, manipulator control equipment and the controller equipment of a mine detection sensor. In failure, in consideration of maintenance nature, correspondence was made possible by module provision. The body became heavier as a result of strengthening, better waterproofing, protection against dust, and bulletproofing. As a result, the target weight limit was set to 1,600kg. The engine power is 39PS, and the hydraulic pressure is 180kg/cm²

The design specification of the sensor arm of MHV is as follows;

- (1) In order to secure horizontal accuracy of position for a wide working range, a horizontal SCARA (Selective Compliance Assembly Robot Arm) robot arm with multiple joints was adopted.
- (2) Reduction gears were made into the planetary rucksack system instead of a harmonic drive to minimize vibration.
- (3) The sensor arm itself has a waterproof level of IP30. For this reason, the whole arm was dressed with the jacket and waterproofing and protection against dust were secured.
- (4) In order to always keep the direction of a mine detection sensor constant, a timing belt was used to move a joint in synchronization with the rotation of the arm..
- (5) The SCARA arm has four-degree-of-freedom. Two-degree-of-freedom are horizontal, one is the perpendicular, and one is the yaw of the sensor. Also they are driven by AC servo motors.
- (6) The maximum payload is 40kg. Each arm length is 80cm. The maximum speed at a tip

is 10 m/min and repetition positioning accuracy is $\pm 1\text{mm}$ in the horizontal direction and $\pm 1\text{mm}$ in the perpendicular direction.

- (7) The maximum payload size is 400mm x 400mm x 400mm, and the SCARA arm full weight is 150kg.
- (8) GPR and a metal detector are installed at the tip of the SCARA arm, with gap control used for the metal detector and gap control used for the GPR.

The system consists of three parts which are control for the main body of MHV, SCARA arm control, and the mine detection sensor. Figures 7 and 8 show the field test in Sakaide city, Kagawa prefecture in March, 2006. Also, the performance of MHV was carried out in March, 2007, Croatia.



Fig. 7. Mine Hunter Vehicle with two manipulator



Fig. 8. Mine detection test of MHV

After this, the controlled metal detector installation schedule on MHV is explained in detail. And then, the current state of development in the anti-personnel mine exposure and clearance system is described, focusing on the robot arm. In particular, we have achieved the reasonable performance of a 6-degree of freedom robot with multi-function tool by means of nonlinear control based on "LOOK AT TABLE" scheme or control theory scheme and also the master-slave hand.

4. Controlled Metal Detector Mounted on Mine Detection Robot

4.1 Overview

Metal detectors are considered as the most reliable sensors for mine detection work. However, landmine detection performance of the metal detectors is highly dependent on the distance between the sensor heads and the buried landmines. Therefore, the landmine detection performance of the metal detectors could be substantially improved if the gap and attitude of the sensor heads can be controlled. In case of robots assisted land mine detection, this function can be performed in a convenient manner where the sensor heads should accurately follow the ground surface maintaining almost uniform gap between the ground surface and the sensor heads by controlling the gap and attitude of the sensor heads. Few mine detection robots that have the capability to recognize ground surface and can control

the gap and attitude of the sensor heads are reported in (Armada, M.A. et al. 2005), (Chesney, R. et al. 2002), (Nonami, K. et al. 2003).

However, to the best of the knowledge of the authors, no research work has been reported in the literature that quantitatively addressed the relationship between the landmine detection performance and controlling the gap and attitude of the sensor head to the ground surface.

The CMD system adopts 3-D stereovision camera rather than LASER scanning as a range sensor because 3-D stereovision camera can capture color information also. Ground of real minefield may have substantial amount of vegetation. Therefore, some image-processing algorithm could be applied with the color images captured by the CCD cameras for recognition of the vegetation to autonomous operation of the CMD in vegetated minefield in future work.

The trajectories are generated by the CMD in such a manner that any obstacle or possible impact with the ground can be avoided. The CMD then tracks the generated trajectories by a trajectory-tracking controller so that the sensor head can follow the ground surface. The effectiveness and the impact related to the gap and attitude control on the mine detection performance of the CMD have been demonstrated by experimental studies.

The rest of the paper is organized as follows. The description of the controlled object has been presented in section 4.2. The kinematic analysis of the CMD has been presented in section 4.3. The description of stereovision camera has been presented in section 4.4. The description of trajectory planning has been presented in section 4.5. The results of experiments of trajectory tracking have been presented in section 4.6. The results of experiments of mine detection have been presented in section 4.7, 4.8. The some conclusions have been presented in section 4.9.

In view of the above, authors' research group has developed a Controlled Metal Detector (CMD) having 3-DOF for any arbitrary positioning of the sensor head. The CMD system can generate 3-D high-speed mapping of the ground surface and can generate trajectories of the sensor head with 3-D stereovision camera. 3-D stereo vision is now being widely used for 3-D mapping and robotics (Clark, F. et al. 2007), (Rochaa, R. et al. 2005), (Xiao, D., et al. 2004) for their powerful sensing capability than other range sensors.

4.2 Controlled Object

The controlled object of this research is called Controlled Metal Detector (CMD). It consists of the two-coil metal detector and a 3-DOF mechanical manipulation mechanism driven by electric motors. The overview of the CMD system is shown in Fig.9. The experimental setup is composed of the main body of the CMD, two PCs, 3-D stereovision camera and a XY-stage as shown in Fig.10. The XY-stage *can perform* the two-dimensional motion in horizontal directions.

The schematic diagram of the CMD is shown in Fig.11. The CMD has 3-DOF composed of three motorized linkages (Link 1, Link 2, and Link 3). The ball screws on these links convert the rotational motion into translation motion. The gyrations of pitch and roll, and movement in vertical direction of the sensor head are performed by controlling the lengths of the Link 1, Link 2 and Link 3. The right-handed coordinate system $\{O_b X_b Y_b Z_b\}$ associated with the CMD is described in Fig.11. The lengths l_1 , l_2 and l_3 (of Link 1, Link 2 and Link 3 respectively) are measured with encoders installed in each link. The calculation methods are described in next section.

The CMD is mounted on the horizontal positioning arm of the XY-stage at the point P_a . Therefore, the point P_a does not move vertically. After the synchronization of the CMD and the horizontal positioning arm of the XY-stage, it is possible to make the sensor head to follow the target trajectories generated with 3-D stereovision data. Moreover, the CMD has no metallic parts within 600 mm from the sensor head; this practically eliminates any chance of interference on the metal detector. Table 1 shows the specifications of the CMD.

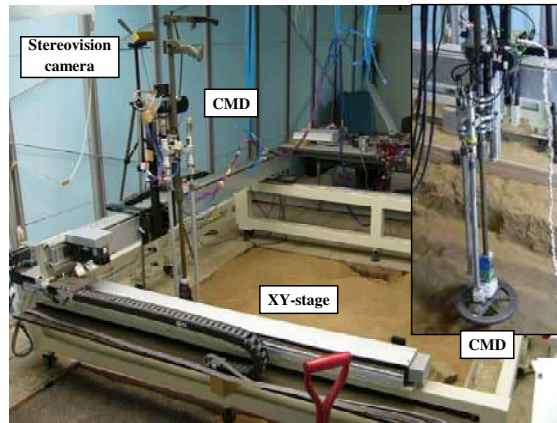


Fig. 9. Overview of CMD system

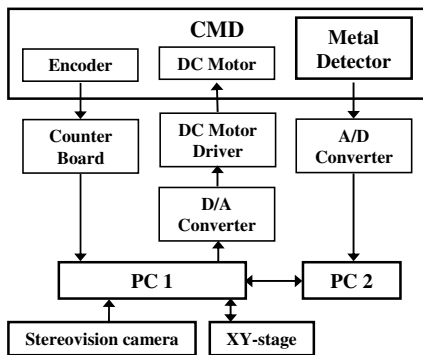


Fig. 10. Architecture of CMD system

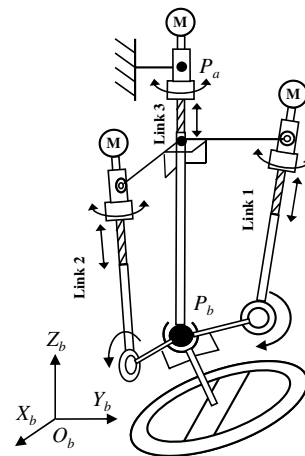


Fig. 11. Configuration of CMD

4.3 Kinematic Analysis

The movements of Link 1 and Link 2 are restrained in the perpendicular plane because there is a ditch on the ball joint P_b . The geometrical relationship between the lengths l_1, l_2 and the

Item	Value	Remarks
Length [mm]	1500	Basic position
Width [mm]	282	
Weight [kg]	10	
Degree of freedom	3	
Stroke speed (max) [mm/s]	100	Link 3
Stroke width [mm]	180	Link 3
Angular velocity (max) [deg/s]	10	Pitch, Roll
Angle range [deg]	± 15	Pitch, Roll
Length of l_4 [mm]	835	
Length of l_5 [mm]	80	

Table 1. Specifications of CMD

pitch angle θ_x , roll angle θ_y of the sensor head shown in Fig. 12 In the CMD system, in order to ensure that the sensor head follows the ground surface without any collision, the trajectory of the attitude of the sensor head and the required change in l_3 are calculated with 3-D vision data. Then the changes in lengths l_1, l_2 are calculated from the inverse kinematics as shown below (1) and (2).

$$l_1 = \sqrt{l_4^2 + 2l_5^2 - 2l_5L \sin(\theta_x + \arctan \frac{l_5}{l_4})} - l_4 \tag{1}$$

$$l_2 = \sqrt{l_4^2 + 2l_5^2 + 2l_5L \sin(\theta_y - \arctan \frac{l_5}{l_4})} - l_4 \tag{2}$$

Moreover, the direct kinematics is as follows.

$$\theta_x = -\arctan \frac{l_5}{l_4} + \arctan \frac{-l_1^2 - 2l_1l_4 + 2l_5^2}{2l_5L} \tag{3}$$

$$\theta_y = \arctan \frac{l_5}{l_4} + \arctan \frac{l_2^2 + 2l_2l_4 - 2l_5^2}{2l_5L} \tag{4}$$

Where l_4 and l_5 are lengths of links, and $L = \sqrt{l_4^2 + l_5^2}$. Moreover, attitude vectors X_s, Y_s of the sensor head are defined as $X_s = [\cos \theta_y, 0, -\sin \theta_y]^T$, $Y_s = [0, \cos \theta_x, \sin \theta_x]^T$ with attitude angles θ_x, θ_y .

4.4 Ground Mapping with 3-D Stereo Vision

The commercial stereovision camera, called Bumblebee (Point Grey Research Inc.), has been used for 3-D stereovision based ground mapping. This stereovision camera uses a parallel stereo method. Table 2 shows the specifications of the stereovision camera. Where the coordinate system consists of: the original point and the Z_c axis are taken the optical center and the optical axis of the left camera, the X_c axis and the Y_c axis are taken the horizontal axis and the vertical axis of the left image, is defined as the camera coordinate system $\{O_c\}$.

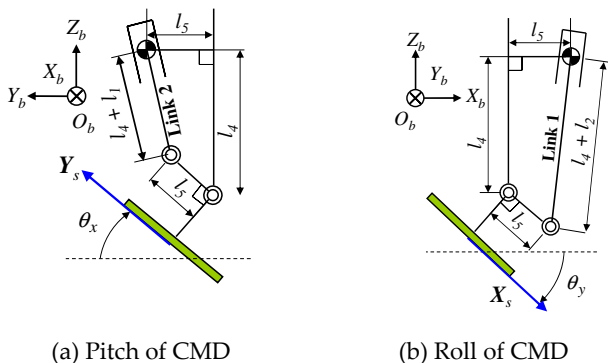


Fig. 12. Geometry of CMD

The stereovision algorithm searches for correspondence points between the left image and the right image acquired with the stereovision camera by the template match. The camera coordinate $[x_c, y_c, z_c]^T$ of point P in the 3-D space is decided from correspondence points p, p' in the right and left images as follows.

$$x_c = \frac{x_l B}{x_l - x_r}, y_c = \frac{y_l B}{x_l - x_r}, z_c = \frac{fB}{x_l - x_r} \tag{5}$$

Where the positions of correspondence points p and p' on the right and left images are defined as $(x_l, y_l), (x_r, y_r)$.

As a result, geographical features information in the camera coordinate system is acquired. Therefore, depth information $f_d(x, y)$ on the ground surface in the base coordinate system is generated with the coordinate conversion. Here a photograph of the detection area as an example is shown in Fig. 13, and the 3-D geographical features map is shown in Fig. 14.

Item	Value
Device size [mm]	160(W)×40(H)×50(D)
Weight [g]	375
Baseline [mm]	120
Focal length [mm]	6
Pixels	320(H) × 240(V)
view angle [deg]	50

Table 2. Specifications of stereovision camera



Fig. 13. Detection area

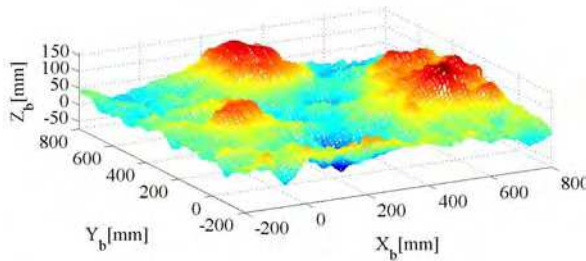


Fig. 14. 3-D mapping

4.5 Trajectory Planning with 3-D Vision Data

The trajectory planning is produced by the off-line. Namely, at first, the 3-dimensional map for the detection area like $1\text{m} \times 1\text{m}$ will be produced by means of the stereovision based image processing, and then, the trajectory planning will be automatically done. The target trajectory has been generated from the depth information acquired with 3-D stereovision. However, the raw depth information from the stereovision camera contains large data volume and also noise. This large volume of data is inconvenient for the trajectory planning. Therefore, a working depth information $f(n_1, n_2)$ has been generated from the original depth information $f_a(x, y)$ provided by the stereovision camera after sampling it at a grid interval d_g . Thus, the working depth information $f(n_1, n_2)$ can be written as:

$$f(n_1, n_2) = f_a(n_1 d_g, n_2 d_g) \tag{6}$$

Where n_1 and n_2 are assumed integers. This working depth information $f(n_1, n_2)$ on the grid has been used in the trajectory planning algorithm.

Figure 15 shows the trajectory of the mounting point P_a of the CMD on landmine detection area ($l_x \times l_y$). The point P_a moves parallel to the $X_b - Y_b$ axis with velocities v_x and v_y respectively. Here, it is necessary to change the velocities of the point P_a depending on the ground surface. However, during the experiment the velocities v_x and v_y are kept equal because of the technical limitations of the XY-stage.

During the trajectory planning, first the position and attitude angles of the sensor head are decided on each grid point of $f(n_1, n_2)$; then these discrete points in the space are connected by straight lines to generate a continuous trajectory. The following objectives are to be satisfied during the trajectory planning:

1. The sensor head keeps itself approximately parallel to the ground surface.
2. The collision between the sensor head and the ground surface is avoided.

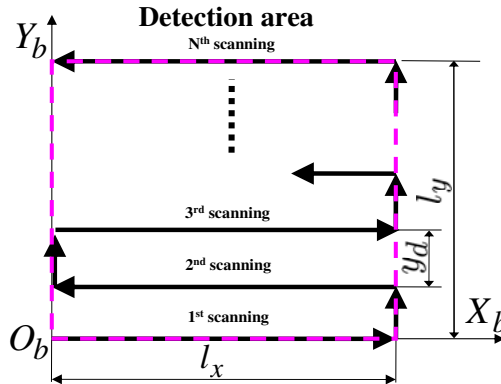


Fig. 15. Trajectory of XY-stage

4.5.1. Decision of Attitude Angles

The target attitude angles θ_x and θ_y of the sensor head that fulfill the first objective stated earlier can be obtained from the depth information as the inclinations of the ground surface. The X_b axial inclination at the grid point (n_1, n_2) of the ground surface is decided by the least square method as follows.

$$\theta_y = \frac{n_s \sum_{i=1}^{n_s} x_i z_i - \sum_{i=1}^{n_s} x_i \sum_{i=1}^{n_s} z_i}{n_s \sum_{i=1}^{n_s} x_i^2 - \left(\sum_{i=1}^{n_s} x_i \right)^2} \tag{7}$$

$$\begin{cases} n_s = (2k_s + 1) \\ x_i = n_1 - k_s + i \\ z_i = f(n_1 - k_s + i, n_2) \end{cases} \tag{8}$$

θ_x is similarly decided. Where k_s is defined as an inclination coefficient of determination. However, the target attitude angles are decided in restrictions. One of the restrictions are is the movable ranges of the mechanism. Another one is the limits of attitude movements θ_{dx} and θ_{dy} between each grid point that consider the passing velocity, v_x and v_y , of the point P_a . The limits of the attitude movements θ_{dx} and θ_{dy} are shown below. Where ω_{MAX} shows the maximum angular velocity.

$$\theta_{dx} = \pm \frac{\omega_{MAX} d_g}{v_x}, \theta_{dy} = \pm \frac{\omega_{MAX} d_g}{v_y} \tag{9}$$

4.5.2. Decision of Length of Link 3

Length l_3 of Link 3 that fulfills the second objective stated earlier is decided with the attitude angles. When the position of the point P_a is $P_a = [n_1 d_g, n_2 d_g, P_{az}]^T$, the position of the center point of the ball joint P_b is $P_b = [n_1 d_g, n_2 d_g, P_{az} - d_z - l_3]^T$. Where the fixed height of the point P_a is assumed to be P_{az} . Moreover, the distance between the point P_a and the point P_b in the

basic stance is assumed to be d_z . Where position S at the center point S on the sensor head's bottom is as follows with attitude vectors X_s and Y_s on each grid point.

$$S = l_s \frac{Y_s \times X_s}{|Y_s \times X_s|} + P_b \tag{10}$$

Where l_s is defined as the distance between the point P_b and the point S . At this time, all the points on the sensor head's bottom keep a distance more than a safety allowance l_{mar} to the ground surface. Therefore maximum length l_3 is decided as filled above. However, l_3 is decided in the restriction of the movable range of the mechanism.

4.5.3. Re-decision of Length of Link 3

Because this trajectory planning targets at minefield, the length l_3 of Link 3 is decided again so that the sensor head does not touch the ground surface in spite of the delay is caused in each response of the Links.

On the i^{th} grid point of the trajectory that XY-stage passes, the position of the point P_a is assumed to be $P_a(i) = [n_1(i)d_g, n_2(i)d_g, P_{az}]^T$, the pitch angle and the roll angle of the sensor head are assumed to be $\theta_x(i)$, $\theta_y(i)$ and the length of Link 3 is assumed to be $l_3(i)$.

In the present research, the CMD does the following three operations at the same time.

1. Attitude changes of the sensor head
2. Vertical motions of the sensor head
3. X_b and Y_b axial motions by XY-stage

Here the length $l_3(i)$ of Link 3 is decided again so that the CMD safely accommodate the time delay caused by these three operations. Here, these three operations are assumed to be completed by the arrival time d_g/v_x , d_g/v_y to the next grid point.

The length $l_3(i)$ is decided again so that all the points on the sensor head's bottom may keep the gap to the depth information on the grid point more than the safety allowance l_{mar} as shown in Fig. 16, evenif the points P_a is at $P_a(i-1)$ and $P_a(i+1)$ with the target attitude angles of the sensor head of the i^{th} grid point. Thus, the collisions with the ground surface caused by the delay of the response can be avoided. However, $l_3(i)$ is decided in the restriction of the movable range of the mechanism and the limits of the expansions l_{dx} and l_{dy} between each grid point that consider the passing velocity, v_x and v_y , of the point P_a . The limits of the expansions l_{dx} and l_{dy} are shown below. Where v_{MAX} is assumed the maximum expansion velocity of Link 3.

$$l_{dx} = \frac{v_{MAX} d_g}{v_x}, l_{dy} = \pm \frac{v_{MAX} d_g}{v_y} \tag{11}$$

Figure 17. shows an example of the generated target trajectory at the center of the sensor head's bottom.

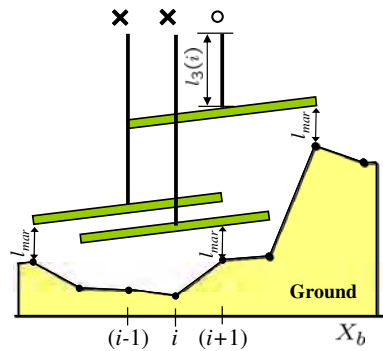
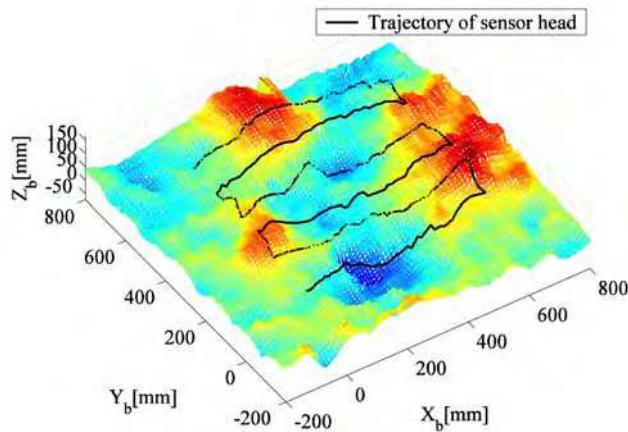
Fig. 16. Decision of l_3 

Fig. 17. Trajectory generation

4.6 Experiments of Trajectory Tracking

The trajectory following experiments of the CMD are conducted over the detection area ($600 \text{ mm} \times 40 \text{ mm}$) shown in Fig. 18. 3-D range information of the detection area is acquired with the stereovision camera in the experiment and the target trajectory is generated using the methods stated earlier. Here each control input to the motor drivers of the CMD is generated with PID controller of feedback control system so that each expansion of the Links follows to the target trajectory. Where the sampling frequency is taken as 50 Hz. Moreover, each gain of the PID controller is shown in Table 3, and each parameter in the trajectory planning is shown in Table 4.



Fig. 18. Detection area for experiment

Link	P	I	D
Link 1	1.5	2.5	0.01
Link 2	3.0	12.0	0.1
Link 3	3.0	12.0	0.1

Table 4. Parameters of trajectory generation

v_x	v_y	y_d	l_{mar}	d_g	k_s
50mm/s	10mm/s	40mm	10mm	10mm	10

Table 3. Gain of PID controller

4.6.1. Experimental Result

Figure 19 showed the generated target trajectory and the result at the center of the sensor head's bottom in the experiment. Fig. 20 showed the time change of the vertical minimal gap between the sensor head's bottom and the ground surface. Fig. 20 shows not real data, but the final data after signal processing in the PC. In addition, these spike peaks are caused by the discrete data like Fig.16. Moreover, the target trajectory and the response of each expansion of Link 1, Link 2 and Link 3 from the experiment beginning for four seconds are shown in Fig. 21.

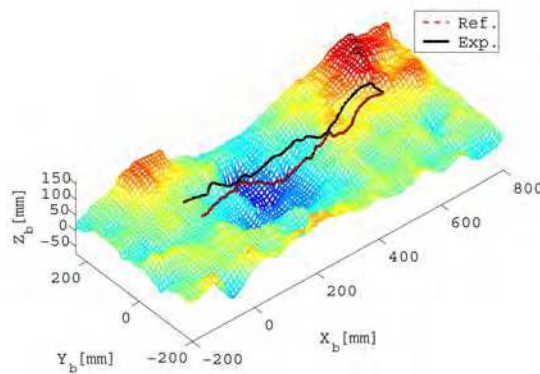


Fig. 19. Trajectory of sensor head

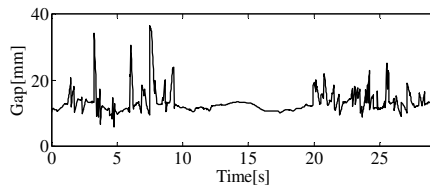
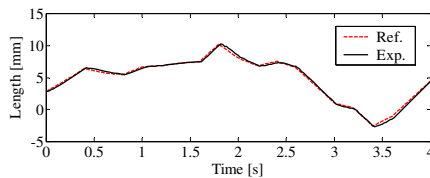
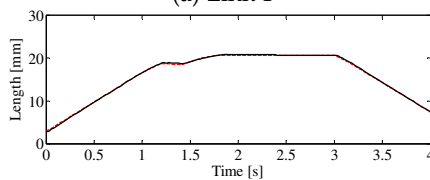


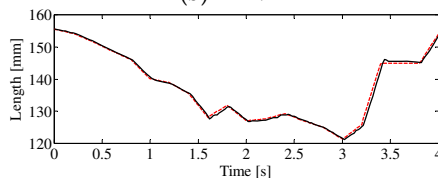
Fig. 20. Gap between sensor head and ground surface



(a) Link 1



(b) Link 2



(c) Link 3

Fig. 21. Trajectory responses of links

4.6.2. Consideration

From Fig. 19, it is obvious that the sensor head follows the generated target trajectory very well. In addition, the sensor head almost keeps the gap more than the safety allowance l_{mar} (Fig. 20) during the detection work, and the trajectory that fulfills the target specifications without contact with the ground surface has been achieved. The safety allowance defined as $l_{mar} = 10$ mm was appropriate in this experiments. Moreover, each link has an excellent trajectory following performance with a small overshoot and delay respectively as shown in Fig. 21.

4.7 Methods of Estimating the Position of Buried Landmines

Estimating the position of the buried landmines with the data of landmine detection sensors is important in detection work by mine detection robots. The metal detector used in this research has a property that the frequency of the output changes before and after the metal

detector mounted on the CMD is passing over a buried metallic object. By using this property, the output signal from the metal detector is converted to a negative value when a landmine exists on the right side from the center of the sensor head along the X_b axis, and to a positive value when a landmine exists on the left side from the center of the sensor head along the X_b axis. The position of the buried landmine is estimated with the processed output of the metal detector.

This section shows the method of estimating the buried position that is confined to the case of the detection area with only one buried landmine. The sensor head is scanned X_b axially in N times in each landmine detection experiment in this research as shown in Fig. 15. In each X_b axially scanning, the strength of the metal reaction: m_i and candidate position of the buried landmine: $[x_i, y_i]$ are decided with the output of the metal detector. After all (N times) scanning finished, the estimated position of the buried landmine is decided with each strength of the metal reaction and each candidate position of the buried landmine as follows.

$$[x, y] = \left[\frac{\sum_{i=1}^N m_i x_i}{\sum_{i=1}^N m_i}, \frac{\sum_{i=1}^N m_i y_i}{\sum_{i=1}^N m_i} \right] \tag{12}$$

Where in the i^{th} scanning, the candidate position of the buried landmine $[x_i, y_i]$ is decided as the middle point of the positions in which the metal reactions pass the threshold $V_d[V]$ or $-V_d[V]$ along the X_b axially with keeping the output increases. In addition, the strength of the metal reaction m_i is assumed a difference between the maximum and minimum values in neighborhood at the candidate position as shown in Fig. 22. Where it is assumed that $V_d = 0.2 V$ and $N = l_y/y_d + 1$ in this research.

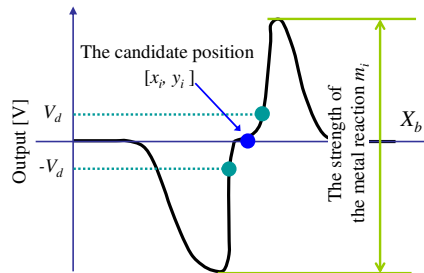


Fig. 22. Definitions of the candidate position (i^{th} scanning)

4.8 Experiments of Mine Detection

Various roughnesses are given to detection area ($l_x \times l_y$) of sands shown in Fig. 18, and the landmine detection experiments by the CMD are conducted. The position of the buried landmine is estimated with acquired data of the metal detector, and effectiveness of the gap and attitude control of the sensor head to landmine detection performance is verified. Here the control method is assumed same to the experiments of trajectory tracking in section 4.6.

4.8.1. Experimental Conditions

Three kinds of trajectories are defined in this experiment to verify effectiveness of the gap and attitude control to landmine detection performance and they are compared. Where Case

Thank You for previewing this eBook

You can read the full version of this eBook in different formats:

- HTML (Free /Available to everyone)
- PDF / TXT (Available to V.I.P. members. Free Standard members can access up to 5 PDF/TXT eBooks per month each month)
- Epub & Mobipocket (Exclusive to V.I.P. members)

To download this full book, simply select the format you desire below

